Design of Backstepping Controller for a Three-phase Shunt Active Filter Interfacing Solar Photovoltaic System to Distribution Grid

1st Jayasankar V N
Department of Electrical & Electronics
National Institute of Technology Karnataka Surathkal
Mangalore, India
jayasankarvn@gmail.com

2nd Vinatha U
Department of Electrical & Electronics
National Institute of Technology Karnataka Surathkal
Mangalore, India
u_vinatha@yahoo.co.in

***Abstract*—This paper presents a controller for a three-phase four-leg shunt active power filter (SAPF), interfacing solar photovoltaic system to distribution grid. The controller consists of a non-linear, robust dc-link voltage control loop based on backstepping algorithm. It also consists of a current harmonic mitigation loop based on dual self tuning filter instantaneous power theory (DSTF-pq theory). The limitations of conventional pq theory based current harmonic mitigation controller are addressed in this paper by employing self tuning filters (STF) to extract the fundamental components of load currents and grid voltages. The effectiveness of the algorithm under steady state and dynamic conditions are comprehensively studied and evaluated in MATLAB/Simulink. The proposed controller is implemented in XC7a35t-cpg236-1 FPGA. The performance of the controller is tested and verified on a laboratory prototype of shunt active power filter.**

***Index Terms*—Shunt active power filter, self tuning filter, pq theory, harmonics mitigation, reference current generation algorithm, dual STF algorithm, extraction of fundamental component**

I. Introduction

The design and implementation of an advanced controller for the grid integration of solar PV systems with the distribution grid is discussed in this paper. The three phase grid interfacing inverter also mitigates the current harmonics in the local non-linear loads. The system consists of a dc-link voltage control algorithm to balance the power flow in the system, and a current harmonic mitigating algorithm. Under sudden and dynamic conditions, the commonly used PI based dc-link voltage controller offers sluggish and imperfect response. Moreover the system stability is not assured by PI controller when large dynamics are present in the dc-link [1]–[3]. A roust, non-linear and stable controller can address these limitations.

Among the existing methods for current harmonic mitigation such as discrete fourier transform (DFT) method, recursive DFT method, fast fourier transform (FFT) method, artificial neural network (ANN) method etc. [4]–[10], the synchronous reference frame (SRF) method and instantaneous active and reactive power (pq) method are predominantly used [1], [2], [11]. The limitations of numerical filters commonly used in SRF and pq methods are the inherent phase delays and inaccurate fundamental component detection [12].

This paper proposes a controller to overcome the limitations of the PI based dc-link voltage controllers. A backstepping controller (BSC) is designed for the dc-link voltage control for the effective control of dc-link voltage under dynamic changes in the power generation and load demand. The Lyapunov stability theorem based step by step design ensures stable operation of the system under sudden and large dynamics in the system. The limitations of SRF and pq based reference current generation methods are addressed in this paper by employing a modified current harmonic mitigation algorithm. This algorithm generates accurate reference current, without any PLL circuits (as required for SRF method). The drawbacks of existing fundamental current detection methods are addressed by using a self tuning filter (STF). The poor performance of pq method under unbalanced and distorted grid voltage conditions is addressed by using self tuning filter for processing the grid voltages before using it for power calculation. The steady state and dynamic simulation studies are conducted using MATLAB-Simulink. The performance of the proposed control scheme is compared with the existing schemes to investigate the improvements achieved by the proposed scheme. A laboratory prototype of shunt active power filter with the proposed control scheme is implemented and verified the effectiveness of the controller experimentally.

II. SAPF interfacing solar PV

The power circuit consists of a three-phase four-leg IGBT inverter shunted with the distribution grid at the point of common coupling (PCC) as shown in fig.1. The non-linear loads are connected at PCC and the solar PV system is connected at the dc side of the inverter. The details of modelling of solar PV system can be referred from [13].

The block diagram of the pq-dual STF control algorithm is shown in Fig. 2. It mainly consists of a backstepping controller for dc-link voltage control and a dual-STF pq controller for current harmonic mitigation.

978-1-5386-9316-2/18/$31.00

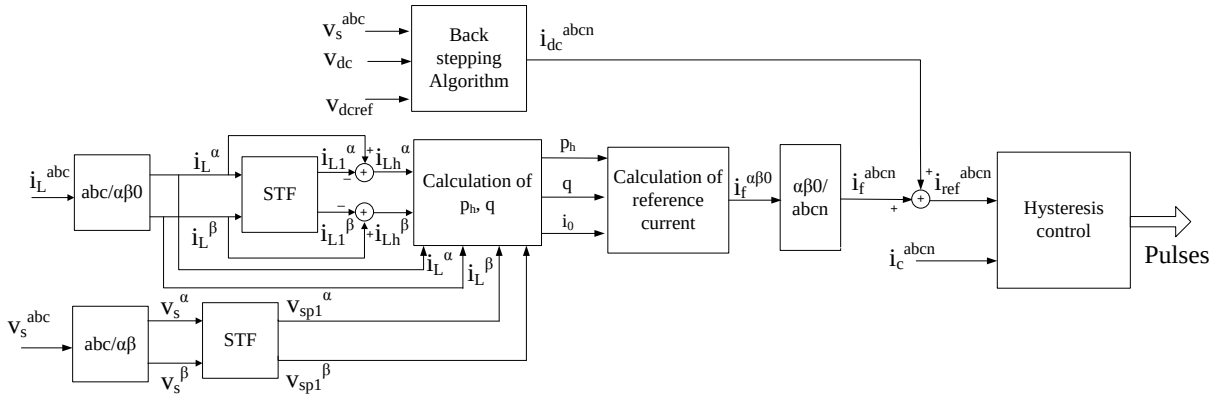

Fig. 2: Shunt active power filter circuit configuration with pq-dual STF control algorithm

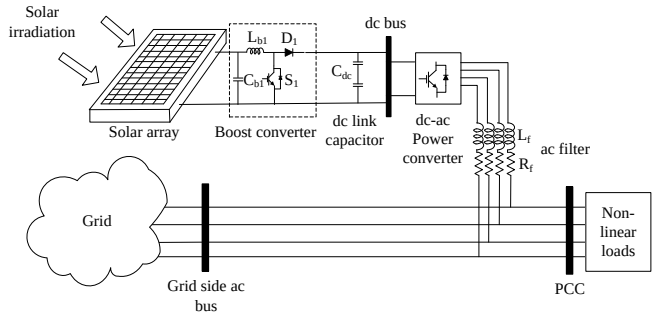

Fig. 1: Shunt active power filter circuit configuration with pq-dual STF control algorithm

A. Current harmonic mitigation using dual-STF-pq algorithm

The load currents and grid voltages are sensed and transformed to $\alpha\beta$ frame using $\alpha-\beta$ transform. The fundamental components of load currents and grid voltages are calculated using self tuning filter (STF). The STF consists of a sinusoidal signal integrator (SSR)with a negative feedback loop, which detects the fundamental component from the input signal with zero phase lag. The transfer function of STF can be written as shown in (1) [14]. The response time and bandwidth of STF is controlled by the sensitivity constant (K). The instantaneous real power needed for harmonic compensation, and instantaneous imaginary power needed for reactive power compensation are calculated using (2) and (3), where $i_{Lh}^{\alpha\beta}$ and $v_{spi}^{\alpha\beta}$ are the harmonic components of load currents and fundamental components of grid voltages in $\alpha\beta$ frame. . The negative sign indicates that the power flow direction is from inverter to PCC [13].

$$H(s)=\frac{K(s+j\omega)+K}{(s+K)^2+\omega^2} \tag{1}$$

$$p_h(t)=-(i_{Lh}^{\alpha}v_{sp1}^{\alpha}+i_{Lh}^{\beta}v_{sp1}^{\beta}) \tag{2}$$

$$q(t)=-(i_L^{\beta}v_s^{\alpha}-i_L^{\alpha}v_s{}^{\beta}) \tag{3}$$

The reference currents for harmonic current mitigation are calculated using (4), where $K_{\alpha\beta}=[(v_s^{\alpha})^2+(v_s^{\beta})^2+(v_s^0)^2]$.

$$\begin{bmatrix} i_f{}^{\alpha} \\ i_f{}^{\beta} \\ i_f{}^0 \end{bmatrix}=\frac{1}{K_{\alpha\beta}}\begin{bmatrix} v_{sp1}^{\alpha} & -v_{sp1}^{\beta} & 0 \\ v_{sp1}^{\beta} & v_{sp1}^{\alpha} & 0 \\ 0 & 0 & K_{\alpha\beta} \end{bmatrix}\begin{bmatrix} p_h \\ q \\ i_0 \end{bmatrix} \tag{4}$$

The reference currents in abc frame (i_{fabcn}) are calculated using inverse $\alpha-\beta$ transform.

B. Control of dc-link voltage

Lyapunov's stability theorem is used for designing back-stepping controller for dc-link voltage control [3]. The control objective is to reduce the voltage tracking error as low as possible. If z is the voltage tracking error, it can be represented as $z=x^*-x$, where x is energy stored in dc capacitor and x^* is the reference value of energy stored in dc link capacitor. The derivative of z can be written as shown in (5). Equation (5) is rewritten as (6), where P_s is the power supplied by the network to maintain the charge in dc link capacitor, P_{sol} is the power injected by solar PV, P_{Rdc} is the losses in leakage resistance of dc link capacitor as represented by (7), (8) and (9) respectively. P_{sw} is the inverter switching loss, which is treated as an unknown parameter. Substituting (8) and (9) in (6), (10) is obtained.

$$\dot{z}=\dot{x^*}-\dot{x} \tag{5}$$

$$\dot{z}=\dot{x^*}-P_s-P_{sol}+P_{Rdc}+P_{sw} \tag{6}$$

$$P_s=v_s^a i_{fdc}^a+v_s^b i_{dc}^b+v_s^c i_{dc}^c \tag{7}$$

$$P_{sol}=i_{dc}\sqrt{\frac{2x}{C_{dc}}} \tag{8}$$

$$P_{Rdc}=\frac{2x}{C_{dc}R_{dc}} \tag{9}$$

$$\dot{z}=\dot{x^*}-P_s-i_{dc}\sqrt{\frac{2x}{C_{dc}}}+\frac{2x}{C_{dc}R_{dc}}+P_{sw} \tag{10}$$

For obtaining a stabilized control law, introducing a Lyapunov function $V=\frac{1}{2}z^2+\frac{1}{2\gamma}\tilde{P_{sw}}^2$, where $\tilde{P_{sw}}=\hat{P_{sw}}-P_{sw}$ is the estimation error of P_{sw} and γ is a positive design parameter.

Differentiating V and substituting $P_{sw} = \hat{P_{sw}} - \tilde{P_{sw}}$ and rearranging, we get (11).

$$\dot{V} = z\left[\dot{x^*} - P_s - i_{dc}\sqrt{\frac{2x}{C_{dc}}} + \frac{2x}{C_{dc}R_{dc}} + \hat{P_{sw}}\right] + \left[\tilde{P_{sw}}(\frac{1}{\gamma}\dot{\tilde{P_{sw}}} - z)\right] \quad (11)$$

For making $\dot{V} <= 0$, equating the terms in square bracket to $-cz$, where c is a positive design parameter. The control law is derived from (11) and shown in (12). The parameter adaptation law derived from (11) is $\dot{\tilde{P_{sw}}} = \gamma z$.

$$P_s = \dot{x^*} - i_{dc}\sqrt{\frac{2x}{C_{dc}}} + \frac{2x}{C_{dc}R_{dc}} + \hat{P_{sw}} + cz \quad (12)$$

From the control law (12), equation (13) can be derived, where X represents phase a,b,c and K_{abc} represents $\left[(v_s^a)^2 + (v_s^b)^2 + (v_s^c)^2\right]$

$$i_{fdc}^X = \frac{1}{K_{abc}}\left[v_s^X\left(\dot{x^*} - i_{dc}\sqrt{\frac{2x}{C_{dc}}} + \frac{2x}{C_{dc}R_{dc}} + \hat{P_{sw}} + cz\right)\right] \quad (13)$$

The reference current for harmonic current mitigation and reference current for dc-link voltage control are added together and applied to hysteresis current controller for generating the pulses for controlling VSI.

III. Simulation Results and Discussion

Numerical simulations are carried out in MATLAB/Simulink platform. The system parameters used in simulation are as follows: Supply Voltage: 3Φ, 400 V (Line–line, RMS), 50Hz, dc link capacitance: 2350 μF, dc link voltage: 700 V, filter Parameters: 5mH, 0.1 Ω, load parameters: Three phase rectifier loaded with 20 Ω, 60 mH. The parameters of the backstepping controller are tuned using trial and error method. For a stable operation, the inequality $c > 2\sqrt{\gamma}$ should be considered while tuning the parameters. The tuned parameters are: γ = 1000 and c = 50. The performance of the backstepping controller is compared with a fast acting PI controller. The transfer function of the fast acting PI controller is given in (14), where, ω_{nv} and ζ are natural frequency of undamped oscillations and damping constant of PI controller respectively.

$$\frac{V_{dc}^2}{V_{dcref}^2} = 2\zeta\omega_{nv}\frac{s + \frac{\omega_{nv}}{2\zeta}}{s^2 + 2\zeta\omega_{nv}s + \omega_{nv}^2} \quad (14)$$

Proportional and integral constants are calculated based on the equation shown in (15). The values of k_p and k_i are selected compromising between fast response time and small overshoot. The tuned values of k_p and k_i are 0.11 and 1.05 respectively.

$$k_p = 2\zeta\omega_{nv}C, k_i = \omega_{nv}^2 C \quad (15)$$

The effectiveness of controller is tested by simulating different system conditions. Both steady state and dynamic conditions are considered for simulation.

A. Steady state condition

Three steady state conditions are considered for simulation: ideal grid voltage condition, unbalanced grid voltage condition and distorted grid voltage condition. The grid current THD before and after compensation under different grid voltage conditions, resulted from three different reference current algorithms are summarized in Table I.

1) Ideal grid voltage: The three phase load currents, grid voltages, compensation currents and grid currents under ideal grid voltage condition are shown in fig.3. A balanced, non-linear load is considered in this case. The load current harmonics are 21.66% in all three phases. It is observed that dual-STF-pq controller effectively mitigates the current harmonics. Accoring to IEEE-519, the permissible current THD level in distribution grid is 5% [15]. The grid current harmonics are 1.22% in all three phases, which are well within the limits. The comparison of dual-STF-pq controller with other existing harmonic mitigation techniques: SRF with numerical low pass filter and pq with numerical low pass filter are given in Table I. The dual-STF-pq method shows superior performance under ideal grid voltage condition.

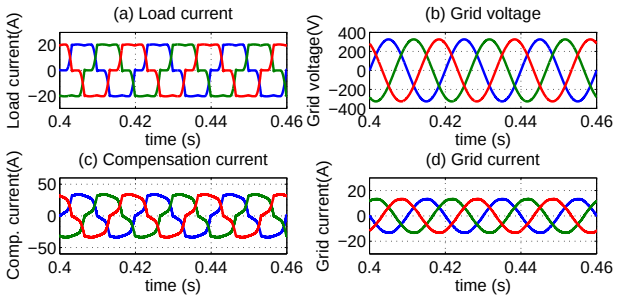

Fig. 3: Simulation results under steady state: (a),(b),(c),(d) load currents, grid voltages, compensation currents and grid currents for case 1

2) Unbalance in grid voltage: Unbalance in grid voltage is simulated with 1.1 pu voltage in phase A and 1 pu voltage in phase B and C. A balanced, non-linear load is considered in this case. The three phase load currents, grid voltages, compensation currents and grid currents under unbalanced grid voltage condition are shown in fig.4. The load current harmonics are 20.40%, 22.26% and 22.47% in A, B and C phases respectively. The grid current harmonics are 1.67%, 1.66% and 1.78% in A, B and C phases respectively. From table I, it is observed that the dual-STF-pq method shows superior performance under unbalanced grid voltage condition also.

3) Distorted grid voltage: 5% distorted grid voltage condition is simulated with 3% of 5^{th} harmonics and 4% of 7^{th} harmonics. A balanced, non-linear load is considered in this case. The three phase load currents, grid voltages, compensation currents and grid currents under distorted grid voltage condition are shown in fig.5. The load current harmonics are 21.67% in all three phases. The grid current harmonics are 1.40% in all three phases. Table I shows that the dual-STF-pq

TABLE I: Performance comparison of current harmonic mitigation algorithms under steady state conditions

Case	Grid current THD (%)								
	Ideal grid voltage			Unbalanced grid voltage			Distorted grid voltage		
	A	B	C	A	B	C	A	B	C
Before compensation	21.66	21.66	21.66	20.40	22.26	22.47	21.67	21.67	21.67
SRF with numerical low pass filter	2.84	2.82	2.81	4.53	4.54	4.50	5.71	5.74	5.73
pq with numerical low pass filter	4.20	4.19	4.19	11.24	9.54	9.82	10.59	10.58	10.58
pq with dual STF	1.22	1.22	1.22	1.67	1.66	1.78	1.40	1.40	1.40

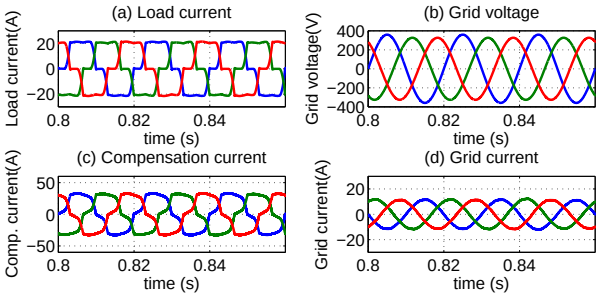

Fig. 4: Simulation results under steady state: (a),(b),(c),(d) load currents, grid voltages, compensation currents and grid currents for case 2

method shows superior performance under 5% distorted grid voltage condition also.

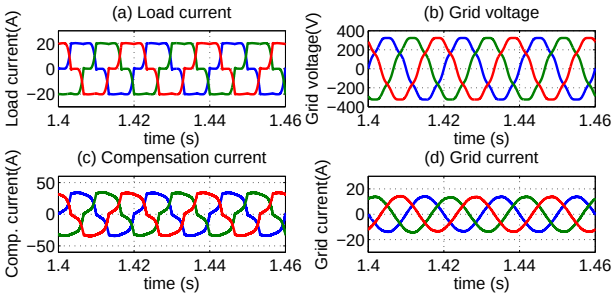

Fig. 5: Simulation results under steady state: (a),(b),(c),(d) load currents, grid voltages, compensation currents and grid currents for case 3

B. Dynamic conditions

Simulation studies are conducted for different dynamic conditions: starting, change in load and change in solar irradiation level. The simulation results under dynamic conditions are summarized in Table II. The rate of improvement in performance of backstepping controller for different dynamic conditions are given in Table III.

1) Starting: The dc-link voltage with PI controller and backstepping controller during starting are shown in fig.6. The integral square error (ISE) and integral time square error (ITSE) of dc-link voltage during starting condition and the steady state grid current THD are listed in Table II. It is observed that the backstepping controller has better dynamic performance compared to PI controller. The steady state performance for both the controllers are found to be similar.

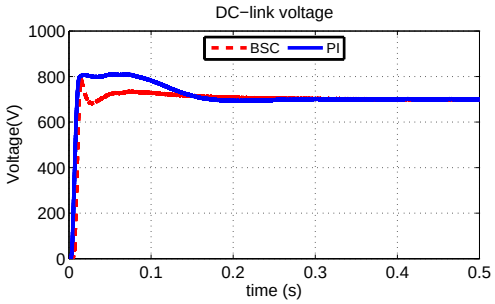

Fig. 6: Simulation results under dynamic state: dc-link voltage waveforms during starting

2) Load change: In this case, the load changes from 25 Ω, 60 mH to 100 Ω, 60 mH. The dc-link voltage with PI controller and backstepping controller during load change are shown in fig.7. From Table II, it is observed that the dynamic performance of backstepping controller is superior to PI controller. Steady state performance is observed as similar.

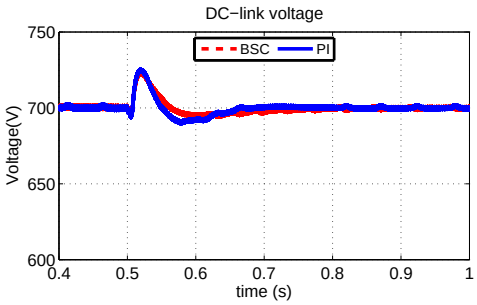

Fig. 7: Simulation results under dynamic state: dc-link voltage waveforms during load change

3) Change in solar irradiation level: In this case, the solar irradiation level change from 600 to 400 W/m^2. The dc-link voltage with PI controller and backstepping controller during load change are shown in fig.8. From the ISE and ITSE values during this condition, it is concluded that the performance of backstepping controller is superior in this condition also.

It is observed from Table I that pq-dual STF algorithm offers better current harmonic elimination in all cases, compared to the algorithms considered. From Table II it can be concluded that backstepping controller offers faster and more effective

TABLE II: Performance comparison of dc-link voltage controllers under dynamic conditions

Case	PI Controller					Backstepping controller				
	Integral square error (ISE) of V_{dc}	Integral time square error (ITSE) of V_{dc}	Steady state grid current THD (%)			Integral square error (ISE) of V_{dc}	Integral time square error (ITSE) of V_{dc}	Steady state grid current THD (%)		
			A	B	C			A	B	C
Starting	8.64×10^{-3}	1.52×10^{-4}	1.54	1.55	1.57	7.76×10^{-3}	5.35×10^{-5}	1.33	1.32	1.34
Load change	3.33×10^{-5}	1.48×10^{-6}	0.56	0.56	0.57	2.85×10^{-5}	1.27×10^{-6}	0.81	0.79	0.80
Irradiation change	4.16×10^{-4}	1.65×10^{-5}	0.88	0.90	0.89	1.12×10^{-5}	3.47×10^{-7}	0.69	0.70	0.70

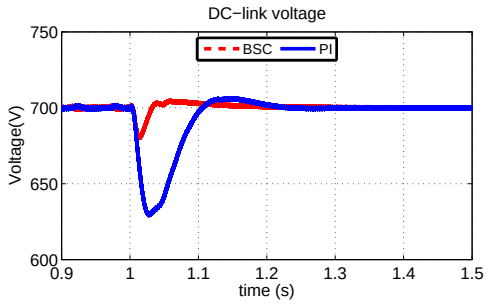

Fig. 8: Simulation results under dynamic state: dc-link voltage waveforms during solar irradiation level change

TABLE III: Rate of improvement in dynamic performance of Backstepping controller

Case	Rate of improvement of Backstepping controller	
	Rate of improvement in ISE (%)	Rate of improvement in ITSE (%)
Starting	10.18	64.80
Load change	14.41	14.19
Irradiation change	97.30	99.79

dc-link voltage control compared to PI control in all three dynamic cases considered. From Table III the rate of improvement in performance of backstepping controller under different dynamic conditions are observed as significantly high.

IV. Hardware Results and Discussion

The proposed control algorithm is implemented in Xilinx (XC7a35t cpg236-1) FPGA. Hall effect sensors LEM LV-25p and LEM LA-55p are used for sensing voltage and current respectively. The IGBT inverter (SKM75GB12T4) with SKYPER 32R gate driver is used for realising shunt active filter. The overall experimental set-up is shown in fig.9. A 30 V, 50 Hz single phase ac source is used as grid. Two series connected 4700 μF capacitors are used as dc link capacitors. DC link voltage reference of 50 V is considered. AC filter parameters are 0.06 Ω and 8.3 mH. Non-linear load used is a single phase rectifier feeding a 10 Ω, 48 mH load.

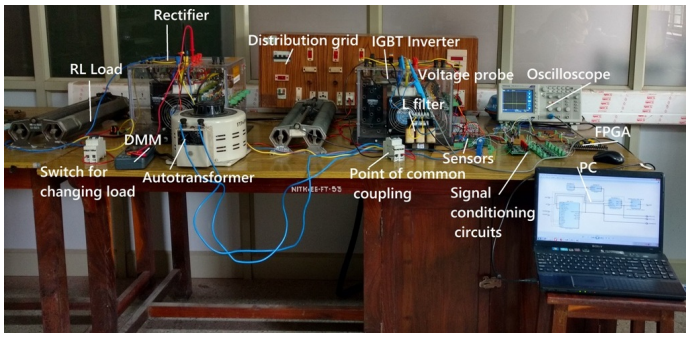

Fig. 9: Laboratory prototype of single phase SHAF

The performance of dual-STF based controller is compared with low pass filter based harmonic mitigation controller. The steady state results under distorted grid voltage condition is shown in fig. 10.

From the harmonic analysis results shown in fig. 11, it is observed that the grid voltage THD is 4% and load current THD is 18.2%. The grid current THDs are 4.2% and 7.5% for dual-STF based controller and LPF-pq controller respectively. It can be concluded that dual STF-pq controller offers superior steady state performance compared to low pass filter based controller.

V. Conclusion

In this paper, a backstepping algorithm based dc-link voltage controller is proposed for the enhanced dynamic performance of SAPF interfacing solar PV system to the distribution grid. An instantaneous power theory based dual STF control (pq-dual STF) algorithm is employed for the current harmonic mitigation. The STF is employed in the reference current generation algorithm to accurately detect the fundamental components with negligible time delay and zero phase shift. The proposed algorithm eliminates the use of PLL circuits for angular position detection of power system. It also eliminates numerical low pass filters from the control system. From the simulation results improved performance is observed compared to conventional PI controller based system under different dynamic conditions. The simulation under steady state conditions shows that pq-dual STF control algorithm has improved the harmonic mitigation performance of SAPF

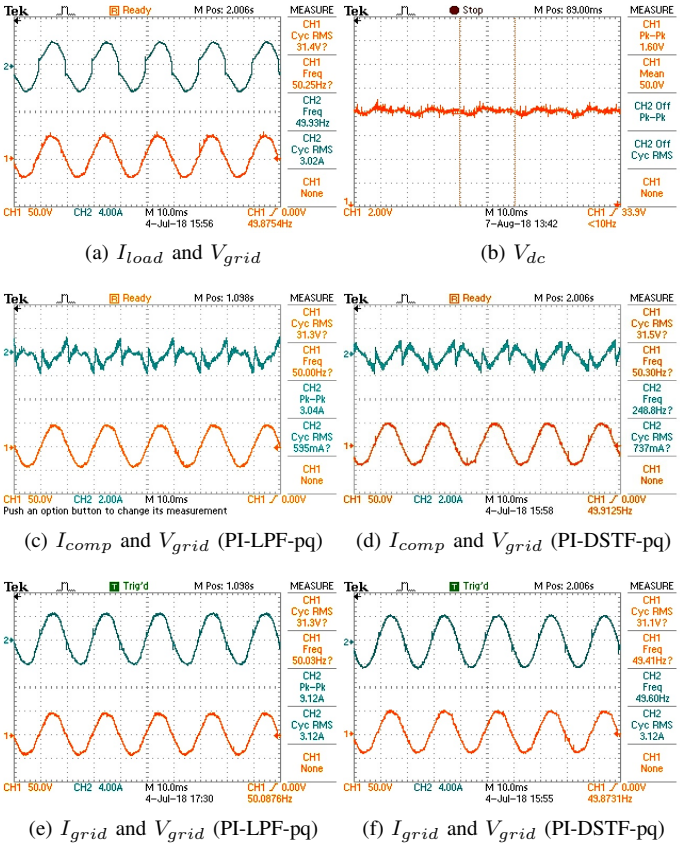

(a) I_{load} and V_{grid} (b) V_{dc}

(c) I_{comp} and V_{grid} (PI-LPF-pq) (d) I_{comp} and V_{grid} (PI-DSTF-pq)

(e) I_{grid} and V_{grid} (PI-LPF-pq) (f) I_{grid} and V_{grid} (PI-DSTF-pq)

Fig. 10: Steady state results under distorted grid voltage with PI-LPF-pq, PI-dualSTF-pq controllers

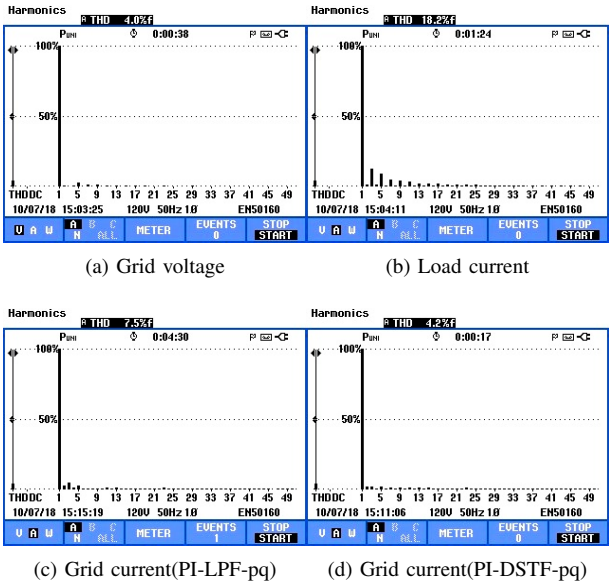

(a) Grid voltage (b) Load current

(c) Grid current(PI-LPF-pq) (d) Grid current(PI-DSTF-pq)

Fig. 11: Harmonic analysis results with PI-LPF-pq and PI-dualSTF-pq controllers

under ideal, unbalanced and distorted grid voltage conditions compared to the existing methods such as SRF, pq with LPF and pq with STF. The steady state simulation results under distorted grid voltage condition are validated experimentally with a laboratory prototype of shunt active power filter.

REFERENCES

[1] H. Akagi, "The state-of-the-art of active filters for power conditioning," in *Power Electronics and Applications, 2005 European Conference on*, 2005, pp. 1–15.

[2] S. Mikkili and A. K. Panda, "Instantaneous active and reactive power and current strategies for current harmonics cancellation in 3-ph 4wire shaf with both pi and fuzzy controllers," *Energy and Power Engineering*, vol. 3, no. 03, pp. 285–298, 2011.

[3] A. Ghamri, T. Mahni, M. Benchouia, K. Srairi, and A. Golea, "Comparative study between different controllers used in three-phase four-wire shunt active filter," *Energy Procedia*, vol. 74, pp. 807–816, 2015.

[4] A. Bagheri, M. Mardaneh, A. Rajaei, and A. Rahideh, "Detection of grid voltage fundamental and harmonic components using kalman filter and generalized averaging method," *IEEE Transactions on Power Electronics*, vol. 31, no. 2, pp. 1064–1073, Feb 2016.

[5] M. Y. Lada, N. I. Zolkifri, J. A. M. Gani, M. R. M. Nawawi, and G. C. Kim, "Reduction of harmonic using single phase shunt active filter based on fft method for cascaded multilevel inverter," in *4th IET Clean Energy and Technology Conference (CEAT 2016)*, Nov 2016, pp. 1–5.

[6] S. Mishra, I. Hussain, B. Singh, A. Chandra, and K. Al-Haddad, "Frequency adaptive pre filtering stage for differentiation based control of shunt active filter under polluted grid conditions," in *2017 IEEE Industry Applications Society Annual Meeting*, Oct 2017, pp. 1–8.

[7] K. C. Patel, A. V. Sant, and M. H. Gohil, "Shunt active filtering with narx feedback neural networks based reference current generation," in *2017 International Conference on Power and Embedded Drive Control (ICPEDC)*, March 2017, pp. 280–285.

[8] B. Chen, G. Pin, W. M. Ng, T. Parisini, and S. Y. R. Hui, "A fast-convergent modulation integral observer for online detection of the fundamental and harmonics in grid-connected power electronics systems," *IEEE Transactions on Power Electronics*, vol. 32, no. 4, pp. 2596–2607, April 2017.

[9] T. D. Raheni and P. Thirumoorthi, "Intelligent control of shunt active power filter for minimization of current harmonics," in *TENCON 2017 - 2017 IEEE Region 10 Conference*, Nov 2017, pp. 2846–2851.

[10] Y. F. Wang and Y. W. Li, "A grid fundamental and harmonic component detection method for single-phase systems," *IEEE Transactions on Power Electronics*, vol. 28, no. 5, pp. 2204–2213, May 2013.

[11] L. Morain and J. Dixon, "41 - active filters," in *Power Electronics Handbook (Third Edition)*, third edition ed., M. H. Rashid, Ed. Boston: Butterworth-Heinemann, 2011, pp. 1193 – 1228.

[12] F. Nejabatkhah, Y. W. Li, and B. Wu, "Control strategies of three-phase distributed generation inverters for grid unbalanced voltage compensation," *IEEE Transactions on Power Electronics*, vol. 31, no. 7, pp. 5228–5241, July 2016.

[13] V. N. Jayasankar and U. Vinatha, "Design of backstepping controller for pv-wind hybrid system with grid-interfacing and shunt active filtering functionality," *International Journal of Power Electronics*, vol. 9, pp. 165–188, 2018.

[14] M. Benchouia, I. Ghadbane, A. Golea, K. Srairi, and M. E. H. Benbouzid, "Implementation of adaptive fuzzy logic and pi controllers to regulate the dc bus voltage of shunt active power filter," *Applied soft computing*, vol. 28, pp. 125–131, 2015.

[15] IEEE, "IEEE recommended practices and requirements for harmonic control in electrical power systems," *IEEE Std 519-1992*, pp. 1–112, April 1993.